

# Transport and noise in resonant tunneling diode using self-consistent Green function calculation

V. Nam Do and P. Dollfus

Institut d'Electronique Fondamentale

Bâtiment 220 – Université Paris Sud, 91405 Orsay cedex, France

V. Lien Nguyen

Theoretical Dept., Institute of Physics, VAST

P.O. Box 429 Bo Ho, Hanoi 10000, Vietnam

## Abstract

The fully self-consistent non-equilibrium Green functions (NEGFs) approach to the quantum transport is developed for the investigation of one-dimensional nano-scale devices. Numerical calculations performed for resonant tunneling diodes (RTDs) of different designs and at different temperatures show reasonable results for the potential and electron density profiles, as well as for the transmission coefficient and the current-voltage characteristics. The resonant behavior is discussed in detail with respect to the quantum well width, the barrier thickness, and the temperature. It is also shown that within the framework of approach used the current noise spectral density can be straightforwardly calculated for both the coherent and the sequential tunneling models. In qualitative agreement with experiments, obtained results highlight the role of charge interaction which causes a fluctuation of density of states in the well and therefore a noise enhancement in the negative differential conductance region.

PACS numbers: 73.63.Hs, 72.70.+m, 73.23.Ad

## I. INTRODUCTION

In nano-scale semiconductor devices the quantum effects become increasingly important and may dominate the transport phenomena. Whatever the system under study the traditional semiclassical Boltzmann equation is no longer an adequate approximation. A rigorous quantum mechanical approach is now necessary not only to study devices intrinsically based on quantum phenomena (e.g. resonant structures), but also to describe more conventional devices as nano scaled field effect transistors where quantum effects cannot be neglected anymore. However, the quantum transport theories are more difficult to implement within a general framework. Among the different quantum formalisms developed during the last decades,<sup>1</sup> the Non-Equilibrium Green Functions can be regarded as one of the most powerful due to its transparent physical route. It provides a general approach to describing quantum transport in the presence of scattering, including the contact and/or gate couplings. A very pedagogical review of the subject can be found in,<sup>2</sup> where the procedure of the self-consistent solution of the Green function and the Poisson equation is properly described. As stated by Christen and Buttiker,<sup>3</sup> the self-consistent treatment of the Coulomb potential is necessary to ensure gauge-invariant current-voltage (I-V) characteristics in non-linear transport.

However, though the formalism is clear, the NEGF-calculation of transport quantities is often technically complicated. Except a few studies realizing the full two-dimensional calculation,<sup>4</sup> it is mostly developed for one-dimensional (1D) transport problems possibly coupled with the two- or three-dimensional description of electrostatics.<sup>5,6,7</sup> The resonant tunneling diode is a typical 1D quantum structure which has been extensively studied both theoretically and experimentally. Although the basic structure of this device is simple, the development of a fully self-consistent NEGF-calculation likely to give reasonable I-V characteristics is still a subject of many efforts.<sup>8,9,10</sup> Alternatively, the Wigner function formalism<sup>11,12,13</sup> or the self-consistent solution of the Schrodinger and Poisson equations<sup>14</sup> have been also used to calculate transport properties of RTDs.

The aim of this work is to present results of the fully self-consistent NEGF-calculation of typical electronic and transport quantities such as potential and electron density profile, transmission coefficient, I-V characteristics, and current noise spectral density in double barrier resonant tunneling structures. The Green functions are calculated exactly within the framework of the tight-binding model and self-consistently coupled with the Poisson

equation. The calculation procedure though standard is formulated in a simple form that can be readily applied to any 1D nano-scale devices and can be easily extended to more complicated structures. Compared to other works in the literature, we obtain a good description of resonant behavior for RTDs of different designs and at different temperatures. Although the NEGF method has been used to calculate the noise in various structures,<sup>15,16</sup> to our best knowledge, the present work is the first attempt to use this formalism to show both sub-poissonian and super-poissonian shot noise in RTDs, which is now the subject of great attention, both theoretically<sup>17,18,19,20,21,22</sup> and experimentally.<sup>23,24,25,26,27</sup>

The paper is organized as follows. Section II describes the model, formulates the problem and the calculation method. In section III the numerical results of the potential and electron density profiles, the transmission coefficient, and the I-V characteristics are presented and discussed in comparison with those reported in the literature. Section IV is specially devoted to the noise calculation. Throughout the work, an attention is properly paid to the practical manner of calculation technique.

## II. METHOD AND FORMULATION

Let us consider a double barrier resonant tunneling device connected to two infinite contacts, the left (L) and the right (R) (Fig. 1). We assume that each contact is characterized by an equilibrium Fermi function,  $f_{L(R)} = 1 / [\exp((E - \mu_{L(R)}) / k_B T) + 1]$ , with a chemical potential,  $\mu_{L(R)}$ . The x-direction is chosen to be perpendicular to the barriers. The (y-z)-cross-section is assumed to be large so that the potential can be considered translation-invariant in this plane. The device is then described by the standard single-band effective mass Hamiltonian:

$$H = H_{jj} + H_z = [E_c - \frac{\hbar^2}{2m_k} \frac{d^2}{dx^2} + U(x)] - \frac{\hbar^2}{2m_z} \frac{\partial^2}{\partial z^2}; \quad (1)$$

which is coupled to two contacts. In Eq. (1),  $E_c$  includes the bottom of conduction band and the conduction-band discontinuities,  $m_k$  ( $m_z$ ) is the longitudinal (transverse) electron effective mass, and  $U(x)$  is the total electrostatic potential. Within the framework of the single particle model, the potential  $U(x)$  can be determined from the Poisson equation:

$$\frac{d}{dx} \left( \frac{dU(x)}{dx} \right) = \frac{e^2}{\epsilon_0} [n_d(x) - n_e(x)]; \quad (2)$$

where  $e$  is the electron charge,  $\epsilon_0$  is the dielectric constant of vacuum,  $\epsilon$  is the relative dielectric constant which may vary along the  $x$ -direction, according to the material, and  $n_e$  and  $n_d$ , respectively, are the electron and donor density, which are assumed to be independent of  $y$ - and  $z$ -coordinates. As usual, we consider the case of fully ionized donors.

In order to solve the Hamiltonian (1) and Eq. (2) self-consistently with respect to the potential  $U$  and the electron density  $n_e$ , taking into account the contact couplings, and further, to calculate the quantities of interest such as the electron density profile and I-V characteristics of the device, it is convenient to use the NEGF method. For the numerical procedure the system under study is spatially meshed and all quantities of interest are computed at the grid sites. For a grid spacing  $a$  along the  $x$ -direction, since the Hamiltonian (1) is already variable-separated, we can write it in the matrix form :

$$H_{ij;k;i^0jk^0} = t_{x-i+1;i^0} (2t_x + U_i + E_{ci} + \epsilon(k))_{ij^0} + t_{x-i-1;i^0} t_{jk^0}; \quad (3)$$

where  $i(i^0)$  indicates grid sites, numbered from left (1) to right ( $N$ ),  $t_x = \hbar^2/2m_k a^2$  is the coupling energy between adjacent sites along the  $x$ -direction (in the nearest neighbor tight-binding scheme), and  $\epsilon(k) = \hbar^2 k^2/2m_\perp$  with  $k$  being the wave vector in the  $(y-z)$ -plane. The Hamiltonian matrix (3) is written in the  $fji > jk > g$ -basis.<sup>2</sup>

Once we have a matrix representation of the Hamiltonian operator it may seem straightforward to get the retarded Green function (GF) by inverting the matrix,  $[(E - i)I - H]^{-1}$ , where  $I$  is the unit matrix and  $i$  is an infinitesimal positive real quantity,  $i \rightarrow 0^+$ . In practical calculations, however, avoiding to work with infinite contacts, the GFs are calculated only in the device domain and the contact couplings are introduced as the 'self-energy' matrices  $\Sigma^r$ . Thus, for the device under study, taking into account the couplings with two contacts, L and R, the retarded GF can be determined as

$$G^r = [(E - i)I - H - \Sigma_L^r - \Sigma_R^r]^{-1}; \quad (4)$$

where  $\Sigma_{L(R)}^r$  is the retarded self-energy matrix describing the coupling between the device and the left (right) contact. Within the framework of the 1D nearest-neighbor tight binding model, these self-energy matrices can be calculated exactly:

$$[\Sigma_{L(R)}^r]_{ij;k;i^0jk^0} = t_x^2 g_{L(R)}(E; k)_{ij^0} t_{jk^0} t_{i^0 i^1(N)}; \quad (5)$$

where  $g_{L(R)}(E; k)$  is a solution of the equation:

$$t_x^2 g_{L(R)}^2 - \Sigma_{L(R)}(E; k) g_{L(R)} + 1 = 0; \quad (6)$$

with the convenient sign for the root. In this equation  $\epsilon_{L(R)}(E; k) = E - \epsilon(k) + 2t_x(U^{(0)} + E_c^{(0)})_{L(R)}$ , where, in the last term,  $E_{cL(R)}^{(0)}$  is the bottom of conduction band at the L(R)-contact and  $U_{L(R)}^{(0)}$  is defined by the applied bias. For instance, if the bias  $V$  is applied to the right contact, then  $U_L^{(0)} = 0$  and  $U_R^{(0)} = V$ .

The advanced GF and the advanced self-energies are Hermitian adjoints of the corresponding retarded matrices:  $G^a = [G^r]^\dagger$  and  $\Sigma^a = [\Sigma^r]^\dagger$ .

In NEGF method the lesser GF plays the central role, in terms of which the measurable quantities are expressed. Noting that in the device under study the contact coupling is the only 'scattering' involved, the lesser GF can be expressed as<sup>2</sup>

$$\begin{aligned} G^<(E; k) &= G^r(E; k) [\epsilon_L^<(E; k) + \epsilon_R^<(E; k) G^a(E; k)] \\ &= i[A_L(E; k)f_L(E) + A_R(E; k)f_R(E)]: \end{aligned} \quad (7)$$

Here, we introduce the lesser tunneling rate defined as  $\epsilon_{L(R)}^< = i[\Gamma_{L(R)}^r - \Gamma_{L(R)}^a]f_{L(R)}(E)$ , and the spectral function  $A_{L(R)} = G^r[\Gamma_{L(R)}^r - \Gamma_{L(R)}^a]G^a$ . As usual,<sup>8</sup> the equilibrium realized in a contact is assumed to be maintained even in the adjacent region of device. The Fermi function ( $f_L$  or  $f_R$ ) with the same chemical potential ( $\mu_L$  or  $\mu_R$ ) can be then applied in the corresponding region (close to L- or R-contact).

Once the lesser GF (Eq. 7) is known it is easy to calculate the electron density:  $[n_e]_i = \frac{1}{i} \int_{-\infty}^{\infty} dE \int dk [G^<]_{ii}$ . Assuming that the vertical effective mass  $m_\perp$  is constant along the  $x$ -direction, the GF  $G^<$  depends on  $k$  only through  $\epsilon(k)$ , the sum over  $k$ -vector can be then changed into an integral that results in

$$[n_e]_i = \frac{m_\perp k_B T}{2\pi^2 a} \sum_{a=L,R} \int_{-\infty}^{\infty} dE \sum_{j=1}^N [A_{a,ij}(E) F_0(-\frac{E}{k_B T})]; \quad i=1,2,\dots,N; \quad (8)$$

where  $F_0$  is the zero-order Fermi-Dirac integral,  $F_0(x) = \ln(1 + e^x)$ .

Thus, basically, the main body of the problem is to solve the Poisson equation (2) and to calculate the electron density (8) self-consistently. Once the self-consistent solution has been found, the current can be calculated as

$$I_i - I = I_0 \int_{-\infty}^{\infty} dE T(E) f F_0(-\frac{E}{k_B T}) - F_0(-\frac{E}{k_B T}) g; \quad (9)$$

Here  $I_0 = (em_\perp k_B T)/(2\pi^2 a)$  and the transmission probability matrix  $T(E)$  is defined as

$$T(E) = \epsilon_L(E) G^r(E) \epsilon_R(E) G^a(E); \quad (10)$$

where  $\Gamma_{L(R)} = i(\Gamma_{L(R)}^r - \Gamma_{L(R)}^a)$  is the tunneling rate.<sup>2</sup>

Before presenting the numerical results we would like to mention that using this self-consistent treatment of the electron interaction, the NEGF approach used in this work becomes equivalent to the scattering Fisher-Lee theory.<sup>1,2</sup> Furthermore, to solve the Poisson equation we use the Newton-Raphson method with a Jacobian to be determined.<sup>10</sup> In this method it is unnecessary to find the Jacobian exactly and a good approximation may be acceptable to reach the convergence. The Jacobian is actually estimated by fitting the electron density resulting from Eq. (8) with the electron density expression  $n_{e,li} = N_c F_{1/2}((\mu_i - U_i)/k_B T)$ , where  $\mu_i$  is the fitting parameter,  $F_{1/2}$  is the Fermi-Dirac integral of order 1/2, and  $N_c$  is the effective conduction band density of states. Using this procedure, both Eqs. (1) and (2) are considered as a single non-linear one for  $U$ , which really reduces the time of calculation.

### III. NUMERICAL RESULTS

The numerical calculations have been performed for typical  $AlGaAs/GaAs/AlGaAs$  RTDs. Two barriers are symmetrical with the height of 0.3 eV and the thickness of  $d = 3$  nm. The width of quantum well is  $w = 5$  nm. The barriers and the quantum well (scattering region) are undoped. The double-barrier structure is embedded between two low-doped buffer layers, each 10 nm -thick. The whole system, in turn, is embedded between two outer access regions of GaAs (emitter and collector), doped at  $10^{18} \text{ cm}^{-3}$ . The thickness of each access region is chosen as 30 nm, which is believed to be large enough (see the inset of Fig. 4). The effective mass is assumed to be constant in the whole device and equal to  $0.067m_0$ , where  $m_0$  is the free-electron mass. The relative dielectric constant of 11.5 is used. This system exhibits one resonant level associated with the conduction band minimum, approximately 0.14 eV above the bottom of conduction band of GaAs, if the band bending is neglected. The temperature is generally chosen to be 300 K. In particular, to check the device-size and the temperature effects, some calculations have been also performed for devices with quantum-well width of 4 nm, with barrier thickness of 2 nm (Figs. 2 and 3), or at temperature of 77 K (Figs. 4 and 5).

Here it should be noted that buffer layers with an appropriate thickness and dopant density are generally used in numerical calculations as well as in experiments.<sup>19,24,27</sup> These layers

yield a reduction of the highest charge density at resonance in the quantum well and of the charge accumulation in the emitter region. Intrinsically such charge accumulations strongly affect the shape of the potential profile and therefore produce a current instability.<sup>20,28</sup> However in this work we limit our investigations to the structures with imperceptible instability.

To model the Hamiltonian (3) the 1D-grid of spacing  $a = 0.25\text{nm}$  is used. With the algorithm mentioned in the preceding section, typically, only 5 iterations are required to reach a self-consistent solution of Eqs. (2) and (8). Fig. 1 (a) shows the potential profile calculated for the device with barriers 3nm-thick and the quantum-well 5nm-wide (hereafter, written for short as  $[\beta=5=3]$ -device) at various applied bias. At zero bias (solid line), the potential is lightly risen around the barriers that pulls the resonant level a bit upward. With an applied bias compared to the resonant one (dashed line) or higher (dot-dashed line), a large portion of the potential drop occurs at the right side of the barriers. Qualitatively, our results of potential profile are similar to those obtained in<sup>8</sup> for the  $[\beta=3=3]$ -device, using the stationary scattering matrix approach. A similar potential profile was also recently reported by Pinaud,<sup>14</sup> solving self-consistently the Schrodinger and the Poisson equations for the  $[\beta=5=5]$ -device.

The electron density profiles, corresponding to the potentials in Fig. 1 (a), are shown in Fig. 1 (b). Clearly, for any bias, in the regions where the total potential is zero, the electron density is precisely given by the donor density. At zero bias the profile is certainly symmetrical. A finite bias brings about an electron accumulation in the well. The accumulation reaches the highest level at the resonant voltage and decreases as the bias is continuously increased. At the same time, the profile becomes more and more asymmetrical. For the bias above resonance, a slight Friedel oscillation of the profile observed in the buffer layer adjacent to the left barrier is due to an electron accumulation at the left barrier, which occurs when the resonant level is much lower than the chemical potential in the left contact. Overall, these results are again in qualitative agreement with those presented in,<sup>14</sup> where however the data for the bias above resonance is not found.

The most profound manifestation of all that are shown in Figs. 1 can be observed in Fig. 2 (a), where the transmission coefficient  $T$  is plotted versus the energy  $E$  for the same device at different applied biases. For low bias (less than or about the resonant bias in I-V characteristics,  $V_p = 0.31\text{V}$ , as can be seen in Fig. 5), the  $T(E)$ -curve exhibits sharp peaks of almost unit on resonance and then falls off rapidly with energy on both sides. In the range

of energy under study we identify two resonant peaks in each  $T(E)$ -curve separated by a distance weakly sensitive to bias and being equal to  $0.24\text{eV}$ . The bias, however, shifts the picture to the left making the first resonant peak to be cut off when the bias becomes higher than the resonant one (the case of  $0.46\text{V}$  in the figure). Such a disappearance of the sharp peak describes the off-resonant state of the device. Certainly, both the width of peak as well as the peak-to-peak distance strongly depend on the device dimensions. In Fig. 2 (b) we compare the  $T(E)$ -curves of three devices slightly different in the barrier thickness or the quantum-well width:  $[3=5=3]$  (solid line),  $[3=4=3]$  (dashed line), and  $[2=5=2]$  (dot-dashed line). In agreement with the data presented in,<sup>14</sup> Fig. 2 (b) reasonably demonstrates that a decrease of either the quantum-well width or the barrier thickness makes the resonant peak wider and the peak-to-peak distance longer. In particular, two devices with the same quantum-well width of  $5\text{nm}$  have the same position of the first resonant peaks, but the peak width is larger and the second peak locates at higher energy for the device with narrower barriers.

In Fig. 3 we show the I-V characteristics for three devices corresponding with the transmission coefficients presented in Fig. 2 (b). To analyze the data in Fig. 3 it is convenient to introduce two quantities:  $I_p$  is the current at the peak and  $r = I_p/I_v$  is the peak to valley ratio, where  $I_v$  is the current at the valley. Then, Fig. 3 demonstrates that a decrease of either the barrier thickness or the quantum-well width results in an increase of  $I_p$ , but a decrease of  $r$  ( $2:3=0.4$ ,  $6:1.4$ , and  $8:3.4$  for  $[3=5=3]$ -(closed circles),  $[3=4=3]$ -(black squares), and  $[2=5=2]$ -(black rhombus)-device, respectively). The latter statement is a consequence of the smearing of the resonant level that broadens the peak of  $T(E)$  as can be seen in Fig. 2 (b). The width of resonance in energy is inversely proportional to the barrier thickness and/or the quantum-well width. That also explains, for example, why two devices with the same quantum-well width of  $5\text{nm}$ , but with different barrier thicknesses, ( $3\text{nm}$  and  $2\text{nm}$ ), exhibit not only strongly different  $I_p$ , but also different resonant biases,  $V_p = 0.307\text{V}$  for  $[3=5=3]$ -(closed circles) and  $0.34\text{V}$  for the other, though the resonant energies are the same, i.e.  $0.14\text{eV}$  (see Fig. 2 (b)).

Concerning the temperature effect we show in Fig. 4 the I-V characteristics for the same  $[3=5=3]$ -device, but at different temperatures,  $300\text{K}$  (closed circles) and  $77\text{K}$  (black squares). As the temperature is lowered from  $300\text{K}$  to  $77\text{K}$ , the current  $I_p$  grows from  $2.28 \cdot 10^5 \text{A cm}^{-2}$  to  $2.62 \cdot 10^5 \text{A cm}^{-2}$ , and simultaneously,  $I_v$  falls from  $0.45 \cdot 10^5 \text{A cm}^{-2}$

to  $0.33 \times 10^5 \text{ A cm}^{-2}$ , which finally produces a large change of the peak-to-valley ratio (from 5 to 8).

As an important note, in the inset of Fig. 4 we compare the I-V characteristics of two devices with the same quantum well width and the same barrier thickness, but with different thicknesses of the GaAs access region, 30nm (closed circles) and 40nm (crosses). It is apparent that two curves are well coincident in the whole range of bias under study. This makes an argument to suggest that, as mentioned in the first section, the GaAs access region of 30nm thick can be considered as large enough and consistent with boundary conditions. Such an access region was used in calculations throughout this work.

#### IV. NOISE CALCULATIONS

In this section we demonstrate how the shot noise can be calculated using the NEGF-code developed in section II. Deviations of the noise from the full (Poissonian) noise value in RTD have been extensively investigated in a great number of works, both theoretical<sup>19,20,22</sup> and experimental.<sup>23,24,25,26,27</sup> Mathematically, the measure of these deviations is the Fano factor  $F$  defined as the ratio of the actual noise spectral density to the full shot noise value  $2eI$ , where  $I$  is the average current. Physically, it is widely accepted that the Pauli exclusion and the charge interaction are the two correlations, which cause observed shot noise deviations. While the Pauli exclusion always causes a suppression of noise, the charge correlation may suppress or enhance the noise, depending on the conduction regime. In RTD, it was experimentally found that the noise is partially suppressed (sub-Poissonian noise,  $F < 1$ ) at low bias voltages (pre-resonance) and becomes very large (super-Poissonian noise,  $F > 1$ ) in the negative differential conductance (NDC) region. From theoretical point of view, typically, there are two approaches based on different descriptions of tunneling process.

Treating the tunneling through RTD as a quantum coherent process, a general expression of noise has been derived.<sup>17,20</sup> In the limit of zero frequency and for two-terminal structures it has the form :

$$S = \frac{e^2}{\hbar} \int_{-\infty}^{\infty} dE \int_{-\infty}^{\infty} dk f T(E_k) \sum_{L,R} f(E) (1 - f(E)) + T(E_k) (1 - T(E_k)) [f_L(E) - f_R(E)]^2 g; \quad (11)$$

where the first term, proportional to  $f(E)(1 - f(E))$ , describes the thermal noise, and the second term, proportional to  $T(E)[1 - T(E)]$ , is nothing but the partition noise. This expression leads to an important consequence that the Fano factor should never be less than 1/2. With  $T(E)$  determined in section II, the noise (11) can be straightforwardly calculated. In the inset of Fig.5 the Fano factor  $F$  calculated in this way for the  $[3=5=3]$ -device is presented in the range of low (pre-resonant) bias  $V$ . It is clear that the obtained  $F(V)$ -dependence describes quite well existent experimental data,<sup>19,24</sup> including a noise suppression in the positive differential conductance (PDC) region close to the resonance. At higher bias, in the NDC region, as critically discussed in 20, the charge interaction becomes to dramatically affect transport properties of the quantum well, and the expression (11) can no longer be used.

On the other hand, treating the tunneling as sequential process in the spirit of master equation, Iannacone et al.<sup>18,19</sup> arrived at the following expression formula for Fano factor:

$$F = 1 - 2g_r = (g_g + g_r)^2; \quad (12)$$

where the generation and recombination rates through barriers are given by

$$g_g^{-1} = (dI_L^{(+)} = dN) / j_t; \quad g_r^{-1} = (dI_R^{(-)} = dN) / j_t; \quad (13)$$

$N$  is the number of electrons in the well at given bias point and  $N$  is the steady-state value of  $N$ , defined from the charge conservation  $I_L^{(+)}(N) = I_R^{(-)}(N)$ . The quantities  $I_L^{(+)}$  and  $I_R^{(-)}$  are here the flux of electrons injected into the well through the left barrier and the flux of electrons leaving the well through the right barrier, respectively. It was reported that<sup>19</sup> the Fano factor calculated from (12) is in good agreement with the experimental data for the  $[12.4=6.2=14.1]$ -sample in a large range of bias, including both the PDC pre-resonant region with a sub-poissonian noise and the NDC region with a super-poissonian noise. To realize a calculation of noise (12), using the NEGF-algorithm developed in section II, we note that the fluxes  $I_L^{(+)}$  and  $I_R^{(-)}$  can be actually expressed as

$$\begin{aligned} I_L^{(+)} &= \int dE \quad A_L(E) [A_L(E) + A_R(E) F_0(\frac{L}{k_B T} \frac{E}{T})]; \\ I_R^{(+)} &= \int dE \quad A_R(E) [A_L(E) F_0(\frac{L}{k_B T} \frac{E}{T}) + A_R(E) F_0(\frac{R}{k_B T} \frac{E}{T})]; \end{aligned} \quad (14)$$

where  $A_{L(R)}$  and  $\Gamma_{L(R)}$  are already defined in eq.(7) and eq.(10), respectively. So, actually, we can also calculate the Fano factor  $F$  (12), using the NEGF-code developed. In Fig.5 we

show  $F$  calculated in this way as a function of bias for the  $[3=5=3]$ -device at two temperatures, 77K (closed circles) and 300K (black squares). Overall, the obtained  $F(V)$ -curves qualitatively resemble experimental data<sup>19,24</sup> with a minimum at the resonant bias and a super-poissonian peak in the NDC region. For a given device, with decreasing temperature, as can be seen in Fig. 5, the minimum becomes deeper (still greater than 1/2) and the super-poissonian peak becomes higher. The dramatic increase of noise observed in experiment<sup>19,24</sup> is caused by the charge interaction enhanced by the particular shape of the density of state in the well. In deriving the expression (12) such an interaction has been self-consistently included. The role of self-consistent Coulomb interaction in creating a super-Poissonian noise is also recently demonstrated by Oriols et al.<sup>22</sup>

Thus, using the NEGF-algorithm developed in section II we are able to calculate the current noise in both tunneling regimes, coherent and sequential. It should be here mentioned that in literature there are different opinions about how a super-Poissonian noise can be produced and its relation to the NDC. In the theory<sup>19</sup> the super-poissonian noise is closely associated with the NDC, when the time  $\tau_g$  (12) is negative. Blanter and Buttiker emphasized the role of current instability and stressed that the bias range of super-poissonian noise is generally different with the NDC range.<sup>20</sup> Comparing the I-V curves and the noises measured in a super-lattice diode and in a RTD, Song et al.<sup>24</sup> concluded that not NDC, but charge accumulation in the well responds for the super-poissonian noise observed in RTD. Safanov et al.<sup>29</sup>, measuring the noise in resonant tunneling via interacting localized states, observed a super-Poissonian noise in the range of bias, where there is no NDC. Authors have also pointed out that the effect on noise of the Pauli exclusion principle and of the Coulomb interaction are similar in most mesoscopic systems. For Coulomb blockade metallic quantum dot structures, studies<sup>30,31</sup> support the idea that not NDC, but charge accumulation in dots, responds for super-poissonian noise. Remarkably, Alekshin et al.<sup>32</sup> recently claimed that while in the sequential tunneling double barrier model the Fano factor  $F$  is still limited by the lowest value of  $1=2$ , in the coherent model  $F$  may drop below this value. Then, authors also suggest that the noise suppression below the value  $1=2$  can be used to identify a coherent transport. Actually, to solve all these, very fundamental, contradictions a more systematic analysis of noise, taking adequately into account the charge interaction is requested. To this end, it is perhaps most convenient to use the NEGF, well-known as the quantum transport approach capable even to deal with far from equilibrium systems.

## V. CONCLUSION

The NEGF approach has been formulated and implemented in a fully self-consistent calculating procedure that can be readily applied to any 1D nanoscale structures and extended to more complicated devices, e.g. nanoscale field effect transistors. The Poisson equation solver routine has been improved to considerably speed up calculations. It yields physically reasonable results and allows us to work in a large range of temperature.

Numerical calculations have been performed for RTDs of different designs and at different temperatures. The potential and electron density profiles obtained for various applied bias, below and above resonance, rationally describe the resonant behavior in the device. The transmission coefficient and the corresponding I-V characteristics seem to be sensitive not only to the quantum-well width, but also to the barrier thickness. Besides the well-known fact that the quantum-well width defines the resonant level, our calculations show that a decrease of either the quantum-well width or the barrier thickness makes the peak of transmission coefficient wider and the peak-to-peak distance longer. Correspondingly, the peak-to-valley ratio in I-V curves decreases, though the value of the current at the peak is considerably risen. The reason merely lies in a broadening of the resonant level, caused by narrowing the quantum-well width and/or the barrier thickness. Additionally, by lowering the temperature from 300K to 77K we observed not only a raise of the peak in I-V curve, but also a reduction of the valley current that leads to a significant increase in the peak-to-valley ratio.

It was also shown that the NEGF-algorithm developed can be straightforwardly used to calculate the current noise in both coherent and sequential tunneling models. In qualitative agreement with experiments, obtained results highlight the role of charge interaction which causes a fluctuation of density of states in the well and therefore a noise enhancement in the NDC region. We believe that in this way, i.e. using the NEGF, a fully quantum transport approach for non-equilibrium problems, one can calculate the noise in a variety of interacting mesoscopic systems and therefore better understand the nature of noise deviations as well as of conduction mechanisms in these structures.

Acknowledgments. This work has been partially done with the support of the European Community under contract IST-506844 (No. ESINANO). One author (V.L.N.) thanks the CNRS for partial financial support under PICS programme No. 404 to his visit at IEF

where this work has been done.

- 
- <sup>1</sup> D.K. Ferry and S.M. Goodnick, *Transport in Nanostructures* (Cambridge Univ. Press, 1997), Chapter 7
  - <sup>2</sup> S. Datta, *Superlattices Microstruct.* 28, 253 (2000) ; *Electronic transport in mesoscopic systems* (Cambridge University Press, 1995), Chapter 8
  - <sup>3</sup> T. Christen and M. Buttiker, *Europhys. Lett.* 35, 523 (1996)
  - <sup>4</sup> A. Svizhenko, M.P. Anantram, T.R. Govindan, and B. Biegel, *J. Appl. Phys.* 91, 2343 (2002)
  - <sup>5</sup> R. Venugopal, M. Paulsson, S. Goswami, S. Datta, and M.S. Lundstrom, *J. Appl. Phys.* 93, 5613 (2003)
  - <sup>6</sup> J. Wang, E. Polizzi, and M. Lundstrom, *J. Appl. Phys.* 96, 2192 (2004)
  - <sup>7</sup> M. Bescond, K. Nehari, J.L. Autran, N. Cavassilas, D. Munteanu, and M. Lannoo, *IEDM, Tech. Dig. IEEE-Cat-No. 04CH37602*, p.617 (2004)
  - <sup>8</sup> W. Potz, *J. Appl. Phys.* 66, 2458 (1989)
  - <sup>9</sup> R. Lake and S. Datta, *Phys. Rev. B* 45, 6670 (1992)
  - <sup>10</sup> R. Lake, G. Klimeck, R.C. Bowen, and D. Jovanovic, *J. Appl. Phys.* 81, 7845 (1997)
  - <sup>11</sup> N.C. Kluksdahl, A.M. Krizan, D.K. Ferry, and C. Ringhofer, *Phys. Rev. B* 39, 7720 (1989)
  - <sup>12</sup> L. Shifren, C. Ringhofer, and D.K. Ferry, *IEEE Transactions on electron devices*, 50, 769 (2003)
  - <sup>13</sup> M. Nedjalkov, H. Kosina, S. Selberherr, C. Ringhofer, and D.K. Ferry, *Phys. Rev. B* 70, 115319 (2004)
  - <sup>14</sup> O. Pinaud, *J. Appl. Phys.* 92, 1987 (2002)
  - <sup>15</sup> A. Levy Yeyati, F. Flores, and E.V. Anda, *Phys. Rev. B*, 47, 10543 (1993)
  - <sup>16</sup> G.H. Ding and T.K. Ng, *Phys. Rev. B* 56, R15521 (1997)
  - <sup>17</sup> Th. Martin and R. Landauer, *Phys. Rev. B* 45, 1742 (1992)
  - <sup>18</sup> G. Iannaccone, M. Macucci, and B. Pellegrini, *Phys. Rev. B* 55, 4539 (1997)
  - <sup>19</sup> G. Iannaccone, G. Lombardi, M. Macucci, and B. Pellegrini, *Phys. Rev. Lett.* 80, 1054 (1998)
  - <sup>20</sup> Ya.M. Blanter and M. Buttiker, *Phys. Rev. B* 59, 10217 (1999)
  - <sup>21</sup> Ya.M. Blanter, M. Buttiker, *Phys. Rep.* 336, 1 (2000)
  - <sup>22</sup> X. Oriols, A. Trois, and G. Bluin, *Appl. Phys. Lett.* 85, 3596 (2004)
  - <sup>23</sup> V.V. Kuznetsov, E.E. Mendez, J.D. Bruno, and J.T. Pham, *Phys. Rev. B* 58, R10159 (1998)
  - <sup>24</sup> W. Song, E.E. Mendez, V. Kuznetsov, and B. Nielsen, *Appl. Phys. Lett.* 82, 1568 (2003)

- <sup>25</sup> M .Tsuchiya and H .Sakaki, Appl.Phys.Lett. 49, 88 (1986)
- <sup>26</sup> N .Nauen, F .Hohls, J.K onen ann, and R J.Haug, Phys.Rev.B 69, 113316 (2004)
- <sup>27</sup> A K M .Newaz, W .Song, and E E .M endez, Phys.Rev.B , 71, 195303 (2005)
- <sup>28</sup> W .Pötz, Phys.Rev.B 41, 12111 (1990)
- <sup>29</sup> S.S Safonov, A K .Savchenko, D A .Bagrets, O N .Jouravlev, Y.V .Nazarov, E H .Lin eld, and D A .R itchie, Phys.Rev.Lett., 91, 136801 (2003)
- <sup>30</sup> V Hung Nguyen, V Lien Nguyen, and Philippe Dollfus, Appl.Phys.Lett. 87, 123107 (2005)
- <sup>31</sup> V Hung Nguyen and V Lien Nguyen, Phys.Rev.B 73, 165327 (2006)
- <sup>32</sup> V.Ya. Aleshkin, I. Reggiani, and M .Rosin , Phys.Rev.B 73, 165320 (2006), anf references therein

FIG .1: Potential profile (a) for the  $[3=5=3]$ -device and corresponding charge density (b) at various applied bias: 0V (solid line), 0.31V (close to resonance, dashed line), and 0.46V (above resonance, dot-dashed line), Temperature: 300K .

FIG .2: (a) Transmission coefficient in logarithmic scale for the  $[3=5=3]$ -device at 300K at the applied bias: 0.31V (dashed line), and 0.46V (dot-dashed line). (b) Comparison the transmission peak of different structures:  $[3/5/3]$  (solid line),  $[3/4/3]$  (dashed line), and  $[2/5/2]$  (dot-dashed line) at  $V = 0.00V$  .

FIG .3: I-V characteristics for the same devices as in Fig.4:  $[3=5=3]$ -(closed circles),  $[3=4=3]$ -(black squares), and  $[2=5=2]$ -(black rhombus); Temperature: 300K .

FIG .4: The temperature effect: 300K (closed circles) and 77K (black squares) for the same  $[3=5=3]$ -device. Inset: the I-V characteristics for two devices with the same quantum -well width and the same barrier thickness,  $[3=5=3]$ , but with different thicknesses of the GaAs access region, 30nm ( ) and 40nm ( ), are compared. Temperature: 300K .

FIG .5: The Fano factor calculated from Eq.(13) is plotted as a function of the applied bias for the  $[3=5=3]$ -device at 300K (black square) and 77K (closed circles). Inset: the Fano factor calculated from Buttiker's formula (11) for the same device at 77K .

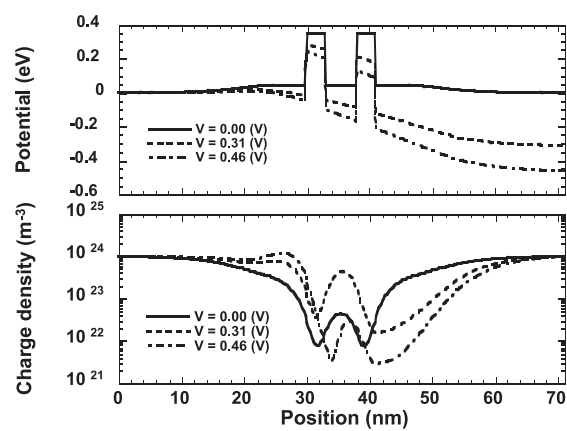


FIGURE 1 (V.Nam DO)

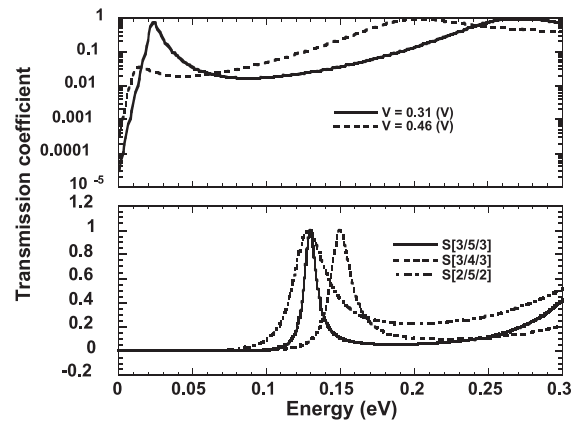


FIGURE 2 (V.Nam DO)

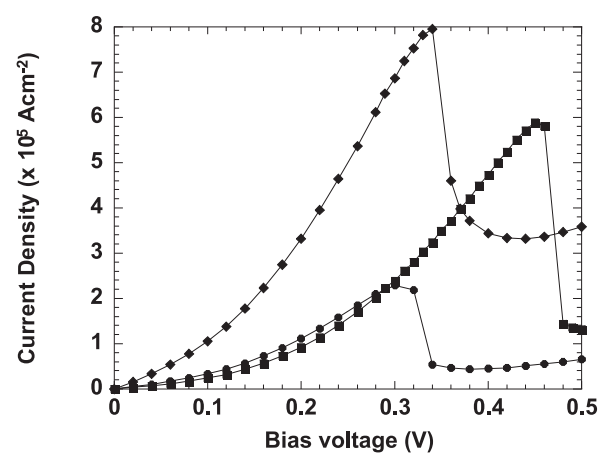


FIGURE 3 (V.Nam DO)

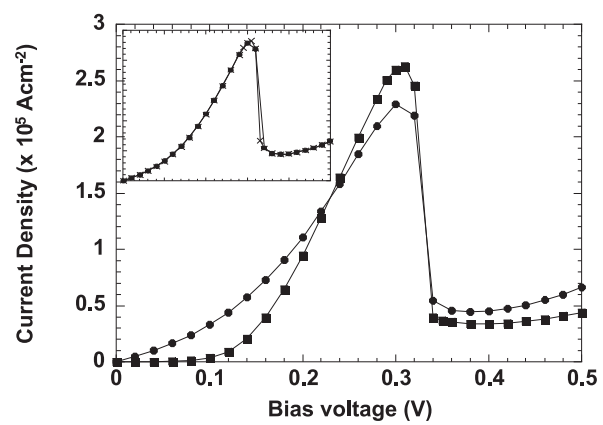


FIGURE 4 (V.Nam DO)

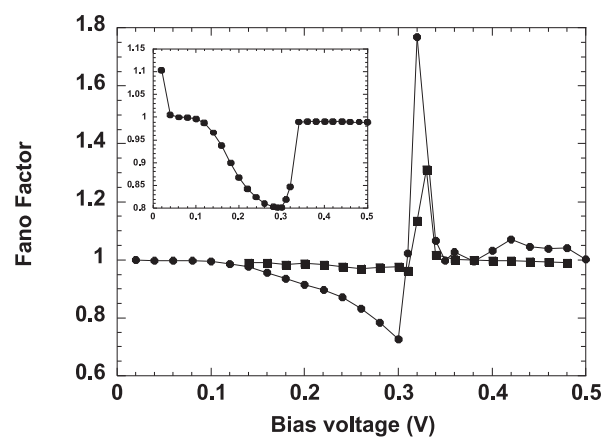


FIGURE 5 (V.Nam DO)